SUPPLEMENTAL MATERIALS

S1: Material and methods

Gravity cores from sites shown in Figure 1 were cut into 1 m long segments and split lengthwise into an archive half and a work half for sampling and geochemical analyses. Pore waters were extracted from the sediments at ambient temperature using a squeezing device operated with argon gas at pressures up to 5 bar. Subsequently, pore waters were filtered through 0.2 µm cellulose acetate membrane filters. Concentrations of sulphate were measured on-board by ion-chromatography (IC, METROHM 761). Acidified subsamples were stored in pre-cleaned vials for shore-based analyses of cations by inductively coupled plasma optical emission spectrometry (ICP-OES, VARIAN 720-ES). All analytical methods applied routinely at GEOMAR are available at http://www.geomar.de or in various publications (Hensen et al., 2007; Scholz et al., 2009).

Sr isotope ratios ($^{87}Sr/^{86}Sr$) of pore water samples were determined according the procedures described in (Schmidt et al., 2019) by thermal ionization mass spectrometry (TIMS, TRITON, ThermoFisher Scientific) at the GEOMAR Helmholtz Centre for Ocean Research Kiel. The measurements were performed after separation of ~1500 ng Sr per sample via ion exchange chromatography using SrSpec resin (Eichrom) at total procedure blanks of < 60 pg. Multiple analyses of NIST SRM 987 provided the base for performance monitoring and normalisation to an $^{87}Sr/^{86}Sr$ value of 0.710248 at a repeatability of ± 0.000007 (2SD, n=5). Most samples performed on comparable accuracy and precision levels. The 2 SE of each TIMS measurement was below ± 0.000010. Multiple analyses of single samples as well as whole procedure duplicates resulted for all samples in 2SD uncertainties < ± 0.000020. As matrix matching standard and reference for modern seawater composition a comparable IAPSO amount was integrated into the sample set and reflect an $^{87}Sr/^{86}Sr$ value of 0.709173 ± 0.000004 (2SD, n=2).

Heat flow was measured on the cruise using the 6 m long Bremen heat flow probe (Villinger et al., 2010). The heat probe is constructed in the classical violin bow design with 21 thermistors distributed over a total length of 5.2 m in a sensor tube. A heater wire for in situ thermal conductivity measurements is also incorporated. The basic processing steps of raw heat flow measurements are outlined in (Hartmann and Villinger, 2002; Villinger et al., 2010). Final heat flow values were calculated by using the in situ measured thermal conductivity when available, otherwise mean values of adjacent measurements.

S2: Locations of GCs in the HAP and mud volcanoes (*italics*).

Location	Station N°	Latitude (N)	Longitude (W)	Water Depth (m)	Core Length (cm)
SFS	M86/5-47 / GC-11	35°47.30'	10°38.53'	4864	468
WFS	M86/5-54 / GC-12	35°49.68'	11°20.79'	4823	466
SFS	M86/5-62 / GC-13	35°47.47'	10°38.44'	4843	211
WFS	M86/5-93 / GC-21	35°49.85'	11°20.20'	4824	444
BFS	M86/5-97 / GC-24	35°47.88'	10°40.76'	4814	482
Reference	M86/5-69 / GC-16	35°42.92'	10°40.94'	4864	399
SWIM 1 East	M86/5-73 / GC-17	35°46.89'	10°34.04'	4853	107
SWIM 1 West	M86/5-92 / GC-20	35°50.08'	11°28.84'	4848	384
WFS (off fault)	M86/5-95 / GC-22	35°50.27'	11°20.72'	4847	304
WFS (off fault)	M86/5-96 / GC-23	35°48.66'	11°20.84'	4859	462
M. Ivanov MV	M86/5-*100 / GC-25*	*35°44.34'*	*10°12.06'*	*4497*	*94*
M. Ivanov MV	M86/5-*24 / GC-4*	*35°44.33'*	*10°12.06'*	*4488*	*238*
Tiamat MV	M86/5-*27 / GC-5*	*35°45.72'*	*10°21.25'*	*4564*	*454*
Abzu MV	M86/5-*28 / GC-6*	*35°45.03'*	*10°19.03'*	*4558*	*475*
Porto MV	M86/5-*8 / GC 1*	*35°33.71'*	*09°30.44'*	*3866*	*195*
Bonjardim MV	*GeoB 9051-2*	*35°27.61*	*09°00.03*	*308*	*263*
Capt. Arutyunov MV	*GeoB 9041-1*	*35°39.70*	*07°19.97*	*1316*	*235*

S3: Locations and results of heat flow measurements in the HAP.

Location	Station N° M86/5-	Latitude (N)	Longitude (W)	Heat Flow (mW m^{-2})
WFS	H1207_P01	35°48.665'	11°20.851'	54.3
	H1207_P02	35°48.980'	11°20.824'	59.0
	H1207_P04	35°49.685'	11°20.762'	74.5
	H1207_P05	35°49.979'	11°20.743'	64.0
	H1207_P06	35°50.274'	11°20.717'	50.4
SFS	H1206_P01	35°47.307'	10°38.506'	55.9
	H1206_P02	35°47.517'	10°38.253'	45.4
	H1206_P04	35°47.941'	10°37.732'	32.9
SWIM Fault	H1208_P01	35°47.192'	10°50.909'	42.0
Central	H1208_P02	35°48.476'	10°51.332'	45.5
Reference	H1205_P01	35°42.931'	10°40.962'	44.7
Reference	H1205_P02	35°42.932'	10°40.964'	44.8

S4: Pore water concentrations of all gravity cores located in the HAP and from ATI mud volcanoes and $^{87}Sr/^{86}Sr$ isotope values of selected samples. Sr-endmember concentrations and corresponding $^{87}Sr/^{86}Sr$ values (*in italics*) at ATI and Porto MVs are from Hensen et al. (2015). Concentrations at Captain Arutyunov MV (CAMV) and Bonjardim MV (*in italics*) are from (Hensen et al., 2007).

Core N°	Sample Depth [cm]	Cl [mM]	SO_4 [mM]	Mg [mM]	Sr [µM]	$^{87}Sr/^{86}Sr$
GC-1	1.5	554.79	28.11	54.59	87.26	
Porto MV	21.5	556.73	27.20	53.02	85.32	
	41.5	556.53	27.37	53.21	86.24	
	61.5	512.66	6.34	41.25	115.92	
	81.5	439.33	0.58	23.78	188.43	
	98.5	397.52	1.45	14.98	241.97	
	118.5	375.82	2.77	11.00	294.59	
	138.5	352.79	0.73	6.47	358.01	
	148.5	350.21	0.43	5.95	389.11	
	158.5	350.99	0.57	5.43	*386.11*	*0.70755*
	168.5	349.93	0.77	5.30	403.06	
	178.5	349.72	0.49	4.97	408.66	
GC-4	1.5	555.98	28.21	53.78	87.84	
M. Ivanov MV	21.5	557.46	28.05	53.66	86.34	
	32.5	556.15	28.31	52.83	85.64	
	42.5	556.30	27.49	52.63	96.23	
	61.5	553.95	20.27	48.44	163.74	
	81.5	541.82	6.56	39.74	258.63	
	101.5	530.56	0.52	32.96	370.25	
	121.5	519.54	0.08	27.45	490.15	
	141.5	508.20	0.63	23.68	587.86	
	161.5	497.88	0.48	19.40	683.23	
	181.5	496.83	2.03	18.36	717.49	
	201.5	483.56	0.45	13.91	803.85	
	211.5	482.22	0.48	13.10	824.26	
	218.5	482.09	0.19	12.59	*830.51*	*0.70759*
GC-5	1.5	558.53	28.06	54.20	87.01	
Tiamat MV	22.0	560.85	27.90	54.12	85.76	
	42.0	560.29	27.97	53.94	86.74	
	72.0	563.52	28.18	53.57	85.57	
	103.0	561.43	26.96	53.01	95.50	
	133.0	556.66	20.19	50.21	146.28	
	163.0	551.62	10.94	46.12	202.22	
	193.0	547.53	2.44	42.60	240.20	
	223.0	538.82	0.18	39.10	307.99	
	253.0	549.14	0.24	36.62	368.77	
	283.0	528.28	0.18	34.11	411.96	
	313.0	521.38	0.16	31.73	456.40	
	343.0	517.92	0.14	29.64	490.41	
	373.0	510.01	0.08	28.13	532.58	
	403.0	501.68	0.07	25.18	546.74	
	423.0	499.39	0.08	24.13	575.96	
	433.0	499.47	0.08	23.20	*546.51*	*0.70771*
GC-6	1.5	560.34	28.28	54.22	85.48	
Abzu MV	22.0	559.73	27.85	53.74	86.59	
	52.0	562.53	28.30	53.71	87.26	
	82.0	560.41	27.23	53.07	97.86	
	112.0	554.59	21.44	49.54	150.16	

Core N°	Sample Depth [cm]	Cl [mM]	SO_4 [mM]	Mg [mM]	Sr [µM]	$^{87}Sr/^{86}Sr$
	142.0	552.35	15.06	45.40	210.03	
	172.0	547.17	9.57	41.86	260.29	
	203.0	539.27	2.99	37.95	315.67	
	233.0	532.98	0.25	34.64	371.27	
	263.0	532.82	0.65	32.24	387.32	
	293.0	526.98	0.54	29.66	439.09	
	322.0	520.35	0.25	27.05	504.67	
	352.0	519.47	0.23	24.89	531.82	
	383.0	514.66	0.27	23.16	569.51	
	413.0	507.05	0.17	20.86	*595.96*	*0.70742*
GC11	1.5	556.67	28.03	53.44	84.07	0.70917
	18.0	562.52	27.73	52.90	84.33	
	32.0	564.25	27.58	52.80	86.14	
	62.0	567.72	27.00	52.58	86.98	
	92.0	564.39	26.12	52.04	88.05	
	122.0	564.25	25.42	51.76	87.71	
	152.0	564.45	24.78	51.34	87.88	
	182.0	561.25	24.07	51.10	88.50	
	212.0	559.19	22.84	50.74	90.09	
	242.0	563.65	22.42	50.29	90.34	
	272.0	560.92	21.50	49.94	91.41	
	303.0	561.51	20.81	49.60	93.43	
	332.0	562.02	20.19	49.36	94.39	
	362.0	563.07	19.61	48.82	94.29	
	392.0	562.24	18.80	48.28	93.16	
	428.0	563.32	17.98	47.47	94.71	
	458.0	557.41	16.74	47.27	96.27	0.70907
GC-12	1.5	560.77	28.46	53.93	86.24	0.70917
	21.5	563.75	27.83	53.59	85.20	
	51.5	563.89	26.73	52.86	86.89	
	71.5	562.18	26.10	52.32	87.02	
	96.5	562.09	25.26	52.04	88.21	
	126.5	560.55	23.53	51.12	88.77	
	158.5	564.92	22.63	50.64	91.20	
	197.5	562.81	21.13	50.10	89.11	
	228.5	568.16	19.77	49.50	88.69	
	258.5	562.66	18.43	48.72	91.34	
	297.5	561.92	17.94	48.90	90.53	
	337.5	558.26	15.27	47.73	94.34	
	377.5	557.58	13.38	46.99	95.21	
	418.5	558.85	11.23	45.98	97.92	
	458.5	562.65	12.41	46.73	100.26	0.70898
GC-13	1.5	565.65	28.61	54.00	85.74	0.70917
	32.0	563.93	27.24	52.88	89.25	
	62.0	564.21	26.14	52.01	94.62	
	82.0	564.26	25.44	51.50	96.23	
	108.0	560.97	24.80	50.92	99.04	
	128.0	-	25.78	54.45	110.93	0.70909
	144.0	568.56	23.03	49.50	102.70	0.70907
	162.0	566.81	21.95	49.23	102.77	
	182.0	567.70	21.03	49.11	105.92	0.70905
	202.0	565.83	20.04	48.82	103.39	
GC-16	2.0	545.24	28.06	54.30	86.13	
	18.5	547.05	27.95	53.78	85.41	
	31.5	547.23	27.87	53.88	87.53	
	61.5	547.44	27.46	53.86	87.21	

Core N°	Sample Depth [cm]	Cl [mM]	SO_4 [mM]	Mg [mM]	Sr [µM]	$^{87}Sr/^{86}Sr$
	91.5	550.76	27.33	53.82	86.87	
	121.5	556.64	27.20	53.62	86.82	
	151.5	547.67	26.37	53.74	86.66	
	181.5	549.19	26.07	53.42	86.35	
	211.5	548.23	25.59	53.08	85.57	
	251.5	543.26	23.76	52.72	85.11	
	291.5	549.69	23.60	52.59	84.90	
	331.5	550.57	23.20	52.55	84.76	
	361.5	554.44	23.06	52.40	84.75	
	391.5	551.03	22.89	52.59	84.90	
GC-17	1.5	557.73	27.75	53.96	85.91	
	8.5	566.43	28.65	54.14	85.67	
	18.5	570.27	28.83	53.62	85.26	
	38.5	566.36	28.40	53.80	86.86	
	58.5	566.32	28.14	53.35	87.39	
	78.5	566.20	28.12	53.61	87.65	
	96.5	566.59	28.18	53.62	87.71	
GC-20	1.0	551.82	27.84	53.99	86.46	
	21.5	555	27.88	53.71	86.73	
	41.5	554.67	27.75	53.57	87.22	
	71.5	556.18	27.31	53.18	86.39	
	102.5	554.28	27.18	53.06	86.37	
	141.5	554.45	26.87	52.85	85.64	
	181.5	558.75	25.82	52.54	85.11	
	211.5	555.67	25.39	52.50	84.11	
	251.5	555.41	24.98	52.22	84.33	
	281.5	560.34	24.84	52.20	84.61	
	311.5	553.62	24.15	51.96	83.37	
	341.5	554.70	23.82	51.90	83.13	
	371.5	552.18	23.02	51.51	83.30	
GC-21	1.5	550.59	28.14	53.99	86.13	0.70918
	31.5	553.84	27.45	53.69	86.67	
	61.5	554.61	26.93	53.12	89.00	
	91.5	551.64	25.92	52.48	90.56	
	121.5	553.70	25.35	51.87	92.07	
	151.5	555.43	24.23	51.57	93.46	
	191.5	553.04	22.85	50.96	95.85	
	231.5	553.64	21.92	50.52	96.57	
	271.5	555.27	20.12	49.66	99.31	
	311.5	553.37	19.51	49.40	101.34	0.70897
	350.5	554.67	18.34	48.84	101.68	
	391.5	552.28	16.73	47.81	103.52	
	411.5	551.85	15.68	47.76	103.85	
	431.5	552.83	15.74	47.76	106.43	0.70891
GC-22	1.5	547.46	28.63	54.18	86.94	
	31.5	549.49	28.23	53.62	85.51	
	61.5	551.95	28.08	52.98	85.85	
	91.5	550.80	27.48	53.18	85.25	
	121.5	554.19	27.06	52.78	84.68	
	151.5	548.22	26.10	52.49	85.21	
	181.5	552.52	25.75	52.27	83.97	
	211.5	553.15	25.16	51.91	83.54	
	241.5	553.03	24.51	51.43	81.76	
	271.5	552.73	23.93	51.19	81.82	
	296.5	551.41	23.21	51.15	81.66	
GC-23	1.5	551.86	27.52	54.34	86.57	

Core N°	Sample Depth [cm]	Cl [mM]	SO_4 [mM]	Mg [mM]	Sr [µM]	$^{87}Sr/^{86}Sr$
	26.5	553.04	27.27	53.68	85.69	
	50.5	556.03	27.19	53.51	85.88	
	80.5	556.38	26.78	53.62	86.18	
	121.5	558.16	25.62	53.18	85.48	
	156.5	558.72	26.48	53.05	85.50	
	191.5	560.44	26.41	53.04	85.68	
	231.5	557.78	25.80	52.78	84.88	
	271.5	560.46	25.58	52.53	84.49	
	311.5	559.69	25.04	52.36	84.07	
	351.5	559.00	24.57	52.21	83.94	
	381.5	558.30	24.21	52.10	83.80	
	411.5	559.12	23.80	52.16	83.97	
	441.5	563.55	23.92	51.99	83.53	
GC-24	2.5	551.49	28.08	54.11	86.00	0.70917
	31.5	551.57	27.28	53.59	88.92	
	61.5	550.43	26.57	53.03	94.26	
	91.5	552.99	26.18	52.43	96.80	
	131.5	551.40	24.87	51.96	101.05	
	171.5	551.77	23.81	51.37	107.12	
	211.5	551.02	22.88	51.28	111.22	0.70890
	251.5	552.79	21.72	50.10	116.68	
	291.5	551.75	20.64	49.65	123.34	
	331.5	550.59	19.12	48.91	128.15	0.70878
	371.5	549.10	18.02	48.23	132.17	
	411.5	547.07	16.90	47.73	137.25	0.70872
	441.5	550.37	16.13	47.43	137.51	
	471.5	555.58	15.45	46.96	138.56	0.70869
GC-25	5.0	544.16	27.47	53.69	93.24	
M. Ivanov MV	21.5	538.05	21.88	49.38	172.99	
	31.5	523.97	2.60	36.91	375.31	
	41.5	507.48	0.42	23.82	644.04	
	51.5	487.74	0.55	14.60	853.65	
	61.5	466.66	0.37	8.05	976.40	
	66.5	449.91	0.91	6.66	*978.95*	*0.70737*
	74.5	508.22	0.80	25.79	606.81	
	83.5	480.09	0.92	12.18	901.83	
GeoB 9041-1	*10*	*570.60 (401.02)* *	*3.52*	*18.07*	*688.04*	
CAMV	*35*	*573.98*	*0.42*	*8.94*	*800.33*	
	60	*573.01*	*0.08*	*7.53*	*810.78*	
	80	*561.42 (199.44)* *	*0.01*	*7.11*	*777.84*	
	105	*585.09*	*0.11*	*7.67*	*830.77*	
	125	*566.25*	*0.05*	*7.13*	*778.38*	
	140	*567.21*	*0.07*	*7.24*	*781.64*	
	160	*595.72 (169.82*)*	*0.07*	*7.93*	*847.43*	
	180	*552.24*	*0.01*	*6.96*	*770.71*	
	195	*585.57*	*0.10*	*7.83*	*835.8*	
	215	*586.54 (164.47)* *	*0.02*	*7.86*	*862.81*	*0.70991*
	230	*571.08*	*0.02*	*7.27*	*811.21*	
GeoB 9051-2	*20*	*542.44*	*24.34*	*41.56*	*100.46*	
Bonjardim MV	*40*	*525.89*	*9.13*	*38.55*	*150.14*	
	60	*-*	*0.95*	*34.27*	*238.09*	
	92	*456.74*	*0.21*	*20.42*	*315.62*	
	112	*430.94*	*0.24*	*18.21*	*370.04*	
	132	*409.77*	*0.16*	*12.92*	*396.61*	
	152	*381.27*	*0.23*	*11.56*	*401.76*	
	172	*345.72*	*0.09*	*8.27*	*392.03*	
	192	*332.09*	*0.12*	*7.35*	*374.95*	

Core N°	Sample Depth [cm]	Cl [mM]	SO_4 [mM]	Mg [mM]	Sr [µM]	$^{87}Sr/^{86}Sr$
	212	*318.94*	*0.10*	*6.05*	*354.82*	*0.70863*

Only chloride values in parentheses for CAMV are shown in Figure 2. These values were recalculated to eliminate the effect of halite dissolution (which has masked the original fluid composition) using ð^{18}O values of pore water samples (Hensen et al., 2007).

S5: Dissolved methane concentrations of gravity cores. CAMV and Bonjardim MV data from (Hensen et al., 2007).

Core N°	Sample Depth [cm]	CH_4 [µM]
GC-1	20	13.31
Porto MV	40	19.02
	43	244.48
	60	3245.57
	80	48.80
	80	49.25
	108	5986.03
	122	1985.91
	131	7137.73
	150	8818.81
	167	5662.02
GC-4	17	0.82
M. Ivanov MV	31	2.92
	31	3.15
	40	7.22
	59	4.31
	77	10.71
	97	1356.86
	117	10741.11
	137	24253.44
	157	4577.75
	177	7184.02
	197	5446.84
	207	6882.54
	215	5344.95
GC-5	17	0.05
Tiamat MV	39	0.23
	68	0.45
	90	1.02
	112	18.34
	129	33.56
	159	211.06
	189	18.25
	210	658.43
	220	4346.78
	240	3774.08
	260	3205.84
	290	4140.62
	309	9973.92
	330	10567.11
	350	5380.78
	368	6750.07
	390	8450.85
	410	10824.69
	430	12055.24
GC-6	15	0.68
Abzu MV	46	0.12
	60	0.38
	76	0.00
	93	1.76
	109	4.17
	130	4.73
	152	7.23
	178	9.40
	196	24.53
	210	433.81
	229	744.23
	247	1184.96
	276	3914.90
	289	1580.79
	320	3898.84
	335	6369.68
	350	9653.61
	370	11325.44
	396	9570.87
	409	8726.57
	429	24810.06
	437	7854.96
	454	5690.72
	460	3053.08
GC11	13	0.00
	24	0.00
	40	0.00
	56	0.00
	86	0.00
	119	0.00
	146	0.00
	166	0.00
	177	0.00
	193	0.00
	208	0.00
	225	0.00
	244	0.00
	270	0.00
	276	0.00
	295	0.00
	309	0.00
	329	0.00
	345	0.00
	359	0.00
	387	0.00
	416	0.00
	424	0.00
	440	0.00
	454	0.00
GC-12	15	0.00
	26	0.00
	47	0.00
	68	0.00
	89	0.27
	118	0.30
	136	0.44
	155	0.52
	177	0.56
	194	0.78
	210	1.11
	225	1.61
	249	2.16
	270	2.07
	284	2.67
	310	2.25
	330	2.38
	344	1.72
	360	4.24
	384	12.75
	404	27.64
	415	38.78

Core N°	Sample Depth [cm]	CH_4 [µM]
	430	22.65
	443	93.17
GC-13	0	0.00
	11	0.00
	40	0.00
	57	0.00
	67	0.00
	87	0.00
	120	0.25
	122	0.07
	132	0.00
	140	0.15
	148.5	0.00
	177	0.04
	198	0.00
GC-16	7	(1.28)*
	23	(0.96)*
	57	(0.22)*
	74	0.01
	110	0.09
	130	0.18
	132	0.00
	155	0.00
	161	0.00
	179	0.00
	208	0.07
	217	0.00
	234	0.00
	248	0.00
	329	0.01
	359	0.06
	389	0.02
GC-17	30	0.31
	47	0.29
	63	0.17
	75	0.12
	93	0.13
GC-20	1	0.06
	10	0.07
	31	0.09
	35	0.08
	89	0.09
	110	0.21
	120	0.19
	136	0.31
	162	0.15
	197	0.28
	210	0.25
	230	0.15
	261	0.35
	277	0.26
	294	0.40
	307	0.34
	326	0.50
	338	0.41
	350	0.40
	364	0.45
GC-21	9	0.00
	28	0.00
	53	0.00
	70	0.00
	87	0.00
	116	0.00
	131	0.00
	149	0.00
	171	0.00
	210	0.00
	227.5	0.10
	244	0.00
	265	0.00
	284	0.03
	307	0.11
	328	0.10
	347	0.14
	378.5	0.20
	389	0.39
	407	0.28
	419	0.72
	428	0.98
GC-22	2	0.06
	12	0.05
	30	0.11
	43	0.12
	65	0.21
	91	0.24
	108	0.30
	117	0.27
	133	0.38
	163	0.32
	194	0.36
	223	0.52
	238	0.55
	276	0.79
GC-23	7	0.00
	21	0.00
	36	0.00
	58	0.00
	76	0.00
	107	0.00
	118	0.00
	136	0.00
	153	0.00
	180	0.00
	212	0.00
	228	0.00
	243	0.00
	266	0.00
	290	0.06
	308.5	0.00
	331	0.08
	349	0.04
	379.5	0.07
	396.5	0.09
	405.5	0.01
	437	0.00
GC-24	7	0.00
	16	0.00
	56	0.00
	67	0.00
	85	0.00
	106	0.00
	126	0.08

Core N°	Sample Depth [cm]	CH_4 [µM]
	147	0.19
	167	0.20
	189	0.31
	208	0.32
	224	0.34
	237	0.77
	256	0.61
	286	0.59
	310	0.79
	327	1.48
	344	1.34
	368	0.13
	382	1.07
	408	1.09
	425	1.45
	443	1.55
	461	1.33
	476	2.48
GC-25	19	17.92
M. Ivanov MV	28	73.85
	48	1577.48
	72	1695.70
	81	1901.75
GeoB 9041-1	15	3017.41
CAMV	29	4164.84
	49	2983.77
	55	3999.91
	85	4436.81
	92	7102.47
	103	3230.42
	123	2582.51
	135	5062.87
	135	3864.63
	148	4330.80
	152	3093.31
	170	3704.40
	187	3560.26
	195	5158.92
GeoB 9051-2	5	13.71
Bonjardim MV	25	22.93
	35	35.51
	49	82.19
	57	569.59
	70	6023.30
	72	1834.64
	95	5821.87
	105	2877.26
	127	2337.20
	134	1128.35
	150	2146.48

*outlier, not considered

S6: Transport-reaction model

Model simulations were carried out using a reactive transport model similar to the one presented by (Hensen et al., 2007) running on Mathematica® Version 12.2. The model considers molecular diffusion and advection of dissolved SO_4, CH_4, Sr, and Mg as well the anaerobic oxidation of CH_4 by SO_4. We applied a general differential scheme of the form:

$$\phi \frac{\delta[C]}{\delta t} = \delta\left(\frac{\phi \cdot D_s \cdot \frac{\delta[C]}{\delta x}}{\delta x}\right) - \frac{\delta(\phi \cdot \upsilon \cdot [C])}{\delta x} + \phi \cdot R \tag{1}$$

where t is time (yr), x is sediment depth (cm), $[C]$ is the concentration of the dissolved pore water species (mmol dm^{-3}), D_s is the diffusion coefficient in the sediments ($cm^2\ yr^{-1}$; corrected for tortuosity; (Boudreau, 1997), ϕ is the sediment porosity (unitless), υ is the net velocity of fluid flow (cm yr^{-1}), and R is a sink/source term for geochemical reactions.

Sediment porosity changes with depth due to sediment compaction. The depth profile is approximated by fitting the measured porosity data with:

$$\phi[x] = (\phi_0 - \phi_z) \cdot e^{-px} + \phi_z \tag{2}$$

where ϕ_z and ϕ_0 are the porosity at the base of each core and at the sediment surface, and p is the attenuation coefficient (cm^{-1}) for the exponential decrease of porosity with depth.

The net velocity of fluid flow (υ) is calculated from the burial velocity of pore water (v_B) and the interstitial fluid flow velocity (ν) induced by upward fluid advection ($\upsilon = \mathrm{v_B} - \nu$):

$$\mathrm{v_B}[x] = \frac{\phi_z \cdot \omega_z}{\phi[x]} \tag{3}$$

$$\nu[x] = \frac{\nu_0 \cdot \phi_0}{\phi[x]} \tag{4}$$

where ω_z is the burial velocity of solids after compaction (cm yr^{-1}) and ν_0 is the intergranular upward fluid flow velocity at the sediment surface (cm yr^{-1}).

D_s ($cm^2\ yr^{-1}$) was determined from the molecular diffusion coefficient (D_0) at bottom water temperature after (Boudreau, 1997):

$$D_S[x] = \frac{D_0[x]}{1 - \ln(\phi)^2} \tag{5}$$

Diffuse fluxes (J) at the sediment surface are calculated from model output according to Fick's first law of diffusion:

$$J_0 = -\phi[x] D_S \frac{\delta[C]}{\delta x} \tag{6}$$

AOM rates (R_{AOM}; in mmol dm^{-3} yr^{-1}) is calculated as:

$$R_{AOM}[x] = k_{AOM} \cdot [SO_4][x] \cdot [CH_4][x] \tag{7}$$

where k_{AOM} is the rate constant (dm^3 mmol^{-1} yr^{-1}).

Increase in temperature (°C) and pressure (bar) with depth are calculated as:

$$T[x] = Temp_I + tempgrad \cdot x \tag{8}$$

$$P[x] = 1 + 0.1 \left(Press_I + \frac{(wds[x] * x)}{100} \right) \tag{9}$$

where $Temp_I$ is the temperature at the sediment surface (°C), *tempgrad* is the temperature gradient (°C cm^{-1}), $Press_I$ is the pressure (bar) at the sediment surface, and *wds* is the density of the wet sediment (g cm^{-3}).

The density of the wet sediment is approximated by:

$$wds[x] = 1.025 * \phi[x] + (1 - \phi[x]) \cdot 2.65 \tag{10}$$

Constant concentrations of dissolved species were prescribed for the upper (measured data for bottom waters) and lower boundary (hypothetical values) of the model column (Dirichlet boundary conditions). Each model was run to steady state starting from arbitrary initial conditions. The upward flow velocities and AOM-rates were determined by fitting the model to the measured pore water concentrations.

S7: Parameters and boundary conditions for model runs of GCs shown in Figure 3B.

Parameter	Symbol	Core number			
		GC 12	GC 13	GC 24	GC 16
Column length (cm)	L	5000	5000	5000	5000

Sedimentation rate after compaction (cm·yr^{-1})	ω_z	0.024	0.024	0.024	0.024
Upward fluid flow velocity at sediment surface (cm·yr^{-1})	v_0	0.038	0.044	0.028	0.0
Porosity (upper boundary)	ϕ_0	0.68	0.71	0.74	0.75
Porosity (lower boundary)	ϕ_z	0.55	0.46	0.57	0.55
Attenuation coefficient (cm^{-1})	q	0.005	0.0067	0.005	0.005
Bottom water temperature (°C)	$Temp_l$	2.5	2.5	2.5	2.5
Temperature gradient (°C cm^{-1})*	$tempgrad$	0.00075	0.0005	0.0005	0.00045
Pressure at sediment surface (bar)	$Press_l$	482	481	481	486
Rate constant of AOM (dm^3 mmol^{-1} yr^{-1})	k_{AOM}	0.0025	0.0045	0.0025	0.0005
Mg-upper boundary (mmol dm^{-3})	Mg_0	54	54	54	54
Mg-lower boundary (mmol dm^{-3})	Mg_z	0	0	0	0
Sr-upper boundary (mmol dm^{-3})	Sr_0	0.086	0.085	0.086	0.086
Sr-lower boundary (mmol dm^{-3})	Sr_z	0.160	0.360	0.560	0.086
SO_4-upper boundary (mmol dm^{-3})	$SO_{4\text{-}0}$	28.5	28.5	28.5	28.1
SO_4-lower boundary (mmol dm^{-3})	$SO_{4\text{-}z}$	0	0	0	0
CH_4-upper boundary (mmol dm^{-3})	$CH_{4\text{-}0}$	1E-06	1E-06	1E-06	1E-06
CH_4-lower boundary (mmol dm^{-3}) = CH_4-solubility at hydrate stability **	$CH_{4\text{-}z}$	74.7	69.1	69.1	68.0

* Calculated by using the closest heat flow measurement available (cf. S3) and a thermal conductivity of the sediment of 1 W K^{-1} m^{-1}.

** Calculated after (Tishchenko et al., 2005) for normal seawater salinity, ambient pressure, and temperature.

S8: Heat flow distortion due to changes in sea floor topography

Distortion of the vertical component of seafloor heat flow due to a step in the basement. This example shows that a 1 km step distorts the vertical component of seafloor heat flow by about ±1 mW m^{-2} that will not be resolved due to measurement errors which are on the order of

±5%. In reality, the step in the basement depth across SWIM1 Fault is much smaller (Martínez-Loriente et al., 2013). Therefore, this example presents an upper bound on the expected distortion.

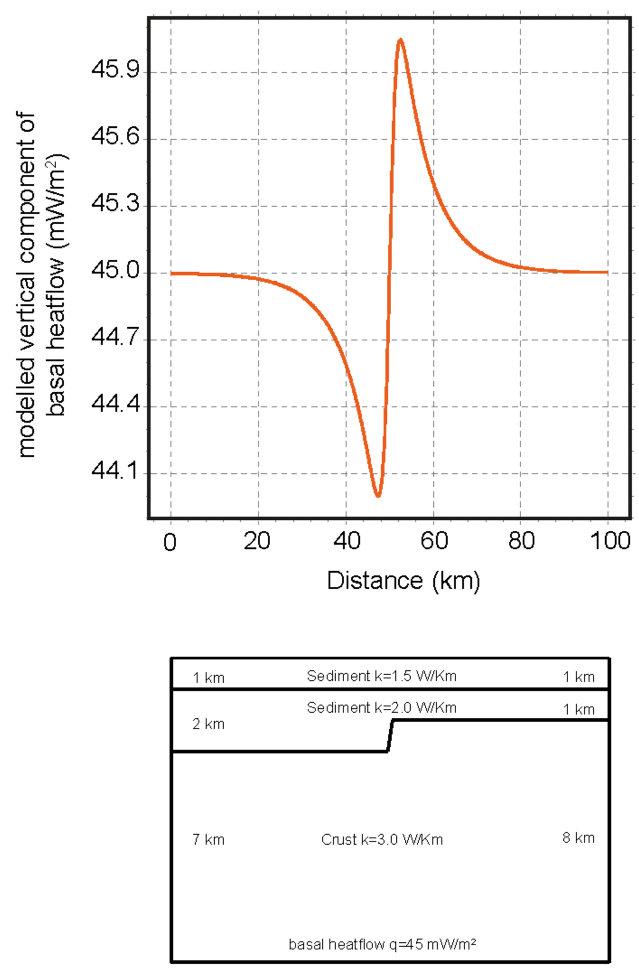

Top: Modelled seafloor heat flow, assuming a basal heat flow of 45 mW m^{-2}.

Bottom: Model dimensions and thermal parameters. The vertical exaggeration is about 1:7.

Heat flow transect across the SWIM1 fault at WFS.

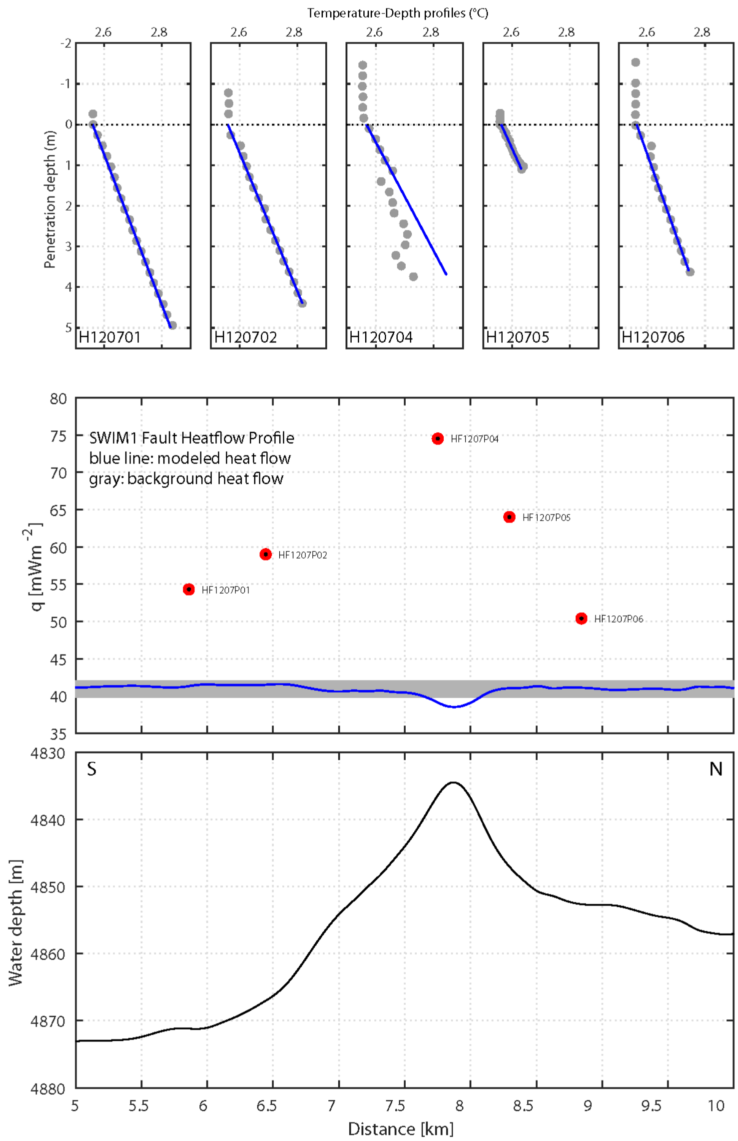

Upper panel: Measured temperature-depth-profiles. It is obvious that the temperature vs. depth on top of SWIM1 is affected by different stages of advective processes.

Middle panel: Heat flow across SWIM1 Fault at WFS (red dots) in comparison to the modelled (expected) heat flow (blue line) due to crustal age and topographic disturbance. The anomaly decays south and north of SWIM1 towards background values. The oceanic crust in this region is assumed to be ~153 Ma old (Müller et al., 2008), which gives an expected lithospheric heat flow of 41 mW m^{-2} (Hasterok, 2013) (grey bar). The width of the gray bar signifies the uncertainty in age.

Lower panel: Bathymetric profile across SWIM1 Fault.

S9: Diffusive fluxes of sulphate, strontium, and magnesium as well as the net upward fluid flow velocity (v_B-v) at the sediment surface. Negative values = downward directed, sediment sink; positive fluxes = upward directed, sediment source.

Location	Station N° M86/5-	SO_4 flux (mmol m^{-2} yr^{-1})	Sr-flux (µmol m^{-2} yr^{-1})	Mg-flux (mmol m^{-2} yr^{-1})	Net upward fluid flow velocity (cm yr^{-1})
WFS	54 / GC-12	-18.60	24.0	-0.99	0.020
WFS	93 / GC-21	-15.79	26.8	-1.84	0.010
SFS	47 / GC-11	-14.24	1.51	-2.45	0.006
SFS	62 / GC-13	-16.84	73.7	-0.13	0.028
LFS	97 / GC-24	-15.41	60.7	-2.12	0.010
Average		-16.18	37.34	-1.51	0.015
Reference	69 / GC-16	-10.22	-10.0	-8.20	-0.018
SWIM1 East	73 / GC-17	-8.95	-0.3	-6.05	-0.013
SWIM1 West	92 / GC-20	-9.66	-12.0	-7.81	-0.012
WFS (off fault)	95 / GC-22	-10.10	-8.9	-5.29	-0.003
WFS (off fault)	96 / GC-23	-11.10	-20.0	-13.2	-0.028
Average		-10.01	-10.44	-8.11	-0.015

REFERENCES

Boudreau, B. P., 1997, Diagenetic models and their implementation: modelling transport and reactions in aquatic sediments, Berlin, Heidelberg, New York, Springer, Berlin, Heidelberg, 414 p.:

Hartmann, A., and Villinger, H., 2002, Inversion of marine heat flow measurements by expansion of the temperature decay function.: Geophysical Journal International, v. 148, no. 3, p. 628--636.

Hasterok, D., 2013, A heat flow based cooling model for tectonic plates: Earth and Planetary Science Letters, v. 361, p. 34-43.

Hensen, C., Nuzzo, M., Hornibrook, E., Pinheiro, L. M., Bock, B., Magalhães, V. H., and Brückmann, W., 2007, Sources of mud volcano fluids in the Gulf of Cadiz—indications for hydrothermal imprint: Geochimica et Cosmochimica Acta, v. 71, no. 5, p. 1232-1248.

Martínez-Loriente, S., Gràcia, E., Bartolome, R., Sallarès, V., Connors, C., Perea, H., Lo Iacono, C., Klaeschen, D., Terrinha, P., Dañobeitia, J. J., and Zitellini, N., 2013, Active deformation in old oceanic lithosphere and significance for earthquake hazard: Seismic imaging of the Coral Patch Ridge area and neighboring abyssal plains (SW Iberian Margin): Geochemistry Geophysics Geosystems, v. 14.

Müller, R. D., Sdrolias, M., Gaina, C., and Roest, W. R., 2008, Age, spreading rates, and spreading asymmetry of the world's ocean crust: Geochemistry, Geophysics, Geosystems, v. 9, no. 4.

Schmidt, C., Hensen, C., Wallmann, K., Liebetrau, V., Tatzel, M., Schurr, S. L., Kutterolf, S., Haffert, L., Geilert, S., Hübscher, C., Lebas, E., Heuser, A., Schmidt, M., Strauss, H., Vogl, J., and Hansteen, T., 2019, Origin of High Mg and SO_4 Fluids in Sediments of the Terceira Rift, Azores-Indications for Caminite Dissolution in a Waning Hydrothermal System: Geochemistry, Geophysics, Geosystems, v. 20, no. 12, p. 6078-6094.

Scholz, F., Hensen, C., Reitz, A., Romer, R. L., Liebetrau, V., Meixner, A., Weise, S. M., and Haeckel, M., 2009, Isotopic evidence ($^{87}Sr/^{86}Sr$, δ^7Li) for alteration of the oceanic crust at deep-rooted mud volcanoes in the Gulf of Cadiz, NE Atlantic Ocean: Geochimica et Cosmochimica Acta, v. 73, no. 19, p. 5444-5459.

Tishchenko, P., Hensen, C., Wallmann, K., and Wong, C. S., 2005, Calculation of the stability and solubility of methane hydrate in seawater: Chemical Geology, v. 219, p. 37-52.

Villinger, H., Tréhu, A. M., and Grevemeyer, I., 2010, Seafloor marine heat flux measurements and estimation of heat flux from seismic observations of bottom simulating reflectors. , *in* Riedel, M., Willough, E. C., and Chopra, S., eds., Geophysical characterization of gas hydrates: Oklahoma, Society of Exploration Geophysicists, p. 279–300.